frontiers in Neuroscience

A Robust Model System for Retinal Hypoxia: Live Imaging of Calcium Dynamics and Gene Expression Studies in Primary Human Mixed Retinal Culture

Shahna Shahulhameed[1], Sarpras Swain[2], Soumya Jana[3], Jay Chhablani[4], Mohammad J. Ali[5], Rajeev R. Pappuru[6], Mudit Tyagi[6], Sushma Vishwakarma[1], Nanda Sailaja[3], Subhabrata Chakrabarti[1], Lopamudra Giri[2], Inderjeet Kaur[1*]

[1]Prof Brien Holden Eye Research Centre, LV Prasad Eye Institute, India, [2]Department of Chemical Engineering, Indian Institute of Technology Hyderabad, India, [3]Department of Electrical Engineering, Indian Institute of Technology Hyderabad, India, [4]School of Medicine, University of Pittsburgh, United States, [5]Govindram Seksaria Institute of Dacryology, LV Prasad Eye Institute, India, [6]Smt. Kanuri Santhamma Center for Vitreo Retinal Diseases, LV Prasad Eye Institute, India

Submitted to Journal:
Frontiers in Neuroscience

Specialty Section:
Neurodegeneration

ISSN:
1662-453X

Article type:
Original Research Article

Received on:
30 Jul 2019

Accepted on:
24 Dec 2019

Provisional PDF published on:
24 Dec 2019

Frontiers website link:
www.frontiersin.org

Citation:
Shahulhameed S, Swain S, Jana S, Chhablani J, Ali MJ, Pappuru RR, Tyagi M, Vishwakarma S, Sailaja N, Chakrabarti S, Giri L and Kaur I(2019) A Robust Model System for Retinal Hypoxia: Live Imaging of Calcium Dynamics and Gene Expression Studies in Primary Human Mixed Retinal Culture. *Front. Neurosci.* 13:1445. doi:10.3389/fnins.2019.01445

Title: A Robust Model System for Retinal Hypoxia: Live Imaging of Calcium Dynamics and Gene Expression Studies in Primary Human Mixed Retinal Culture

Shahna Shahulhameed[±1], Sarpras Swain[±2], Soumya Jana[3], Jay Chhablani[4], Mohammad Javed Ali[5], Rajeev R Pappuru[6], Mudit Tyagi[6], Sushma Vishwakarma[1], Nanda Sailaja[3], Subhabrata Chakrabarti[1], Lopamudra Giri*[2], Inderjeet Kaur*[1]

[1]Prof Brien Holden Eye Research Centre, LV Prasad Eye Institute, Hyderabad, India
[2]Department of Chemical Engineering, Indian Institute of Technology, Hyderabad, India
[3]Department of Electrical Engineering, Indian Institute of Technology, Hyderabad, India
[4]Medical Retina and Vitreoretinal Surgery, University of Pittsburgh School of Medicine, Pittsburgh, USA
[5]Govindram Seksaria Institute of Dacryology, LV Prasad Eye Institute, Hyderabad, India
[6]Smt. Kanuri Santhamma Center for Vitreo Retinal Diseases, LV Prasad Eye Institute, Hyderabad, India
[±]Shahna Shahulhameed and Sarpras Swain should be considered joint first author.
*Inderjeet Kaur and Lopamudra Giri should be considered joint corresponding author.

E-mail address of authors:
Shahna Shahulhameed: shahna135@gmail.com
Sarpras Swain:ch14resch01002@iith.ac.in
Soumya Jana: jana@iith.ac.in
Jay Chhablani: chhablanijk2@upmc.edu
Mohammad Javed Ali:javed@lvpei.org
Rajeev R Pappuru: rajeev@lvpei.org
Mudit Tyagi: drmudit@lvpei.org
Sushma Vishwakarma:svishwakarma17@gmail.com
Nanda Sailaja:ee14mtech11007@iith.ac.in
Subhabrata Chakrabarti: subho@lvpei.org

CORRESPONDENCE

Inderjeet Kaur
Prof Brien Holden Eye Research Centre, LV Prasad Eye Institute, Hyderabad, India,
inderjeet@lvpei.org, Tel. no. +91- 40-30612508, Fax no. +91-40-23548271

Lopamudra Giri -Department of Chemical Engineering, Indian Institute of Technology, Hyderabad, India, giril@iith.ac.in Tel. no. +91-40-23017024 Fax no.+91-40-23016032

Abstract

The detailed mechanisms underlying oxidative stress leading to neuroinflammation and neurodegeneration in retinal vascular conditions including diabetic retinopathy, retinopathy of prematurity etc. remains largely unexplored mainly due to lack of suitable disease models that can simulate the inherent neuron-glia interactions in human retina. Specifically, establishment of a mixed retinal culture containing both neuron and glial cell types remains a challenge due to different conditions required for their optimal growth and differentiation. Here, we establish a novel primary mixed retinal culture (MRC) model system containing neurons, astrocytes, Müller glia and microglia from human donor retina that can be used to study the neuromodulatory effects of glial cells under the stress. The cell characterization based on immunostaining with individual cell types specific markers and their presence in close vicinity to each other further underscores their utility for studying their crosstalk. To the best of our knowledge, this is the first instance of an *in vitro* model obtained from human donor retina containing four major cell types. Next, we induce hypoxic stress to MRC to investigate if hypoxia activated neuro-glia modulates altered gene expression for inflammatory, apoptotic and angiogenic markers and Ca^{2+} transients by live cell imaging. Further, we performed *k*-means clustering of the Ca^{2+} responses to identify the modification of clustering pattern in stressed condition. Finally, we provide the evidence that the altered Ca^{2+} transient correlates to differential expression of genes shown to be involved in neuro-inflammation, angiogenesis and neurodegeneration under the hypoxic conditions as seen earlier in human cell lines and animal models of diabetic retinopathy. The major features of the hypoxic conditions in the proposed human MRC model included: increase in microglia activity, chemokine and cytokine expression and percentage of cells having higher amplitude and frequency of Ca^{2+} transients. Thus, the proposed experimental system can potentially serve as an ideal *in vitro* model for studying the neuroinflammatory and neurodegenerative changes in retina and identifying newer drug targets.

Keywords: retina, glia, calcium spiking, neurons, hypoxia, neurodegeneration, inflammation

Introduction

Neuro-glia interactions in the retina are known to play a crucial role for maintaining retinal homeostasis. Abnormalities in glial cell activation disrupts the homeostasis leading to inflammation, neovascularization and compromised retinal functions thereby causing neurodegenerative diseases such as ROP, AMD, glaucoma and diabetic retinopathy. Cytosolic calcium (Ca^{2+}) plays a key role in regulation of homeostasis in retina and its waves are known to maintain glia-astrocyte, astrocyte-astrocyte, as well as astrocyte-neuron communication. Generally, glial cells are present in close contact with the neurons and the neuronal activity has been shown to induce rise in intracellular Ca^{2+} levels in glia (Newman, 2005). While Ca^{2+} signaling has been studied in primary cultures of rat retina, mouse tissue slices and pig retina (Pereira Tde et al., 2010; Rosa et al., 2015; Agte et al., 2017), a systematic and quantitative analysis of it in human retina with multiple cell types remains elusive. Specifically, there is a paucity of cell-based models to obtain the baseline functionality in form of Ca^{2+} spiking patterns in primary human retina including both glial cells and neurons. Furthermore, retina being a highly complex 3D structure with multiple cell types arranged in a well-defined pattern, it is rather challenging to establish an *in vitro* disease model for drug screening studies. Therefore,

recent studies focus on optimization of culture conditions for culturing of two or more cell types in order to simulate complex *in vivo* situation (Skytt et al., 2016; Park et al., 2018).

Ca^{2+} signaling in glial cells is known to be significantly altered for various eye diseases (Pereira Tde et al., 2010; Crish and Calkins, 2011). Specifically, in case of neurodegeneration, the increased in basal Ca^{2+} level and augmented Ca^{2+} transients in astrocytes cause neurotoxicity (Kuchibhotla et al., 2009). It has also been indicated that the activation of microglia and associated increase in Ca^{2+} flux may kill the neurons, as observed in mouse retinal degenerations (Yu et al., 2015; Zhao et al., 2015). An increased level of oxidative stress and inflammation in retinal microenvironment often enhances retinal neurodegeneration under varied retinal pathology (Rohowetz et al., 2018). Hence, the effect of hypoxia has gained considerable interest as a mediator of retinal injury and inflammation (Arden and Sivaprasad, 2011). While the increase in Ca^{2+} under hyperglycemic conditions is known to cause neurodegenerative conditions (Shin et al., 2014), there are limited investigations on the study of hypoxia mediated modulation of Ca^{2+} dynamics in retina.

In general, the existing studies on hypoxia in retina are restricted in mice (Brahmachari et al., 2006; Rosa et al., 2015) and pig (Hainsworth et al., 2002; Acharya et al., 2017), and none of these provides a suitable model for studying the human retina (Hartung, 2008). The studies on immortalized cell lines are usually derived from tumor cells that suffer from the loss of original tissue specificity and phenotypes with multiple passages (Matteucci et al., 2015). While there are independent investigations on primary cultures of Müller (Puro, 2002), astrocytes (Barber et al., 2000), microglia (Ibrahim et al., 2011), there are limited investigations focusing on co-culturing them together. The rationale behind developing such a co-culture model containing multiple glial cell types stems from the fact that the microglia-Müller glia cross-talk act as a critical mechanism in the modulation of retinal response to injury in the mouse models (Arroba et al., 2014).

The major challenge in generating a model for studying retinal neurodegeneration includes the inherent heterogeneity in cellular activity and induction of neuroinflammation through activation of microglia and astrocytes. Hence, we aim to to establish a primary mixed retinal culture (MRC) model containing neuron, astrocytes, microglia and Müller glia resembling the major cellular composition of human retina. Further, in order to identify their interactions and changes in pattern in calcium dynamics under hypoxic condition, we proposed to study the collective responses through time lapse calcium imaging. Thus, in order to obtain a statistical model for the heterogeneity present in mixed retinal culture, we performed clustering of Ca^{2+} transients obtained from primary mixed retinal cell culture under normal and oxidative stress conditions. Similar approaches of clustering and classification of Ca^{2+} spiking was implemented to study the effect of GPCR targeting drugs on Ca^{2+} response for rat hippocampal neurons (Swain et al., 2018).

First, we show that the proposed *in vitro* system contains four major types of retinal cells in the culture. We further assessed if there is change in gene expression profiles under hypoxia and found significantly differential expression of proinflammatory and angiogenic genes and cytokines. Consistent with the previous studies on rat/human retina, our proposed model demonstrated increase in IBA1 and GFAP protein levels and increased expression for *HIF-1α, CXCR4, IL1-β* and *VEGF*. Further, this work shows that the clustering of calcium dynamics is significantly modulated under hypoxia. It also reveals that hypoxia induces increase in percentage of hyperactive cells that correlate with the activation of microglial cells obtained

from spatial mapping of IBA1 expression in the mixed population. Our model shows reproducibility in gene expression and clustering pattern of Ca^{2+} response across different cultures obtained from various human subjects. Thus, the co-culture model presented here can be regarded as a robust model for retinal hypoxia that can be used for studying the pathological mechanisms involved in various retinal vascular and neurodegenerative condition.

Materials and methods

Preparation of human mixed retinal cell cultures

The study adhered to the tenets of declaration of Helsinki and was approved by institutional review board, LV Prasad Eye Institute, Hyderabad. Donor retina from cadaver as well as from patients due to conditions such as staphyloma and open globe injury were used to establish a primary mixed retinal cell culture system. The cadaveric donor eyes were collected (within 24 hours of death) in a sterile moist glass bottles from Ramayamma International Eye Bank, LV Prasad Eye Institute and washed with sterile PBS containing 2X concentrations of Penicillin and Streptomycin. The retinal tissues were removed using a pair of sterile forceps from the donor eye by making a posterior cut and washed gently with 1X PBS. The enucleated eyeballs from patients were collected after obtaining the written informed consent and immediately transported to the lab on ice. The retina was removed from these eye balls as similar to the cadaveric eyes. The retinal tissues collected from either of the sources were washed gently with 1X PBS to remove the RPE and choroid pigments. The tissue was then chopped in to small pieces using a sterile surgical blade. The chopped tissues were again washed with 1X PBS and treated with 1X trypsin EDTA (0.25%) for a period of 15-20 min at 37˚C. Trypsin activity was arrested by adding complete DMEM (DMEM+10% FBS+1% Penicillin-streptomycin) and centrifuged at 1000rpm for 3min. The dissociated pieces were collected and resuspended in 2ml PBS and gently triturated with P1000 pipette tip to further obtain a suspension of cells. The suspensions of the cells were then passed through a 70micron size cell strainer to remove undigested pieces of tissues if any. The cells were collected after the centrifugation and resuspended in DMEM containing 10% serum and 1% antibiotics. The cells were seeded in a sterile tissue culture grade T-75 mm flask and kept undisturbed for seven days under standard cell culture conditions followed by changing medium at every three days.

Immunofluorescence for retinal cell characterization

Immunofluorescence was done to characterize the cells in mixed retinal culture. Briefly, the cells (approximately 5000 cells/mL) were seeded on a sterile glass coverslip and allowed to attain 70-80% confluency. The cells were fixed with 4% formaldehyde in PBS for 10 min at room temperature. The cells were washed with 1X PBS and permeabilized with 0.5% Triton X-100 in PBS for 10 min. This was followed by incubation with blocking buffer consisting of 2% BSA in PBS for 1 hour at room temperature. The primary antibodies were diluted with blocking buffer and added to the cells for overnight incubation at 4˚C. The primary antibodies were used for identification of cells in the mixed retinal cultures including mouse anti-ionized calcium-binding adaptor molecule 1 (IBA1;for microglia, Abcam, Catalog No. ab178680), rabbit anti-glial fibrillary acidic protein (GFAP; for astrocytes, Catalog No. Dako, Z0344), rabbit anti nestin (for neuronal progenitor cells, Millipore, Catalog No. ABD 69), rabbit beta-III tubulin (β-III tubulin;

for neurons, Abcam, Catalog No. ab18207) and rabbit anti glutamine synthetase (GS; for Müller glia, Abcam, Catalog No. ab176562). The cells were washed thrice with 1X PBS followed by incubation for 45 min at room temperature with secondary antibodies (diluted in blocking buffer) Alexa flour 488 conjugated anti rabbit (Life Tech, Catalog No. A11008), Alexa flour 594 conjugated anti rabbit (Life Tech. Catalog No. A11012) and Alexa flour 594 conjugated anti mouse (Life Tech. Catalog No. A11005). The cells were washed thrice with 1X PBS, mounted with Slow fade gold antifade containing DAPI (Life Technologies, Ref. S36939) and scanned using EVOS fluorescent microscope.

Cell viability estimation and Hypoxia induction

The cells from earlier passages (P1 & P2) were used for the experiment. The cell viability was estimated using Alamar blue dye-based assay using different concentrations of $CoCl_2$ (Sigma Aldrich, Catalog No. C-8661-25G). Briefly, 2000 cells were seeded on a 96-well plate and allowed to attain 70-80% confluent. Prior to the exposure of stress, the complete DMEM was replaced with serum free medium and incubated for 6 hours. The cells were then treated with 100 µM and 150 µM $CoCl_2$ for inducing hypoxia for a period of 24 hours in serum free medium. 10 µL of Alamar blue reagent (Life Technologies, Catalog No. DAL1025) was added on to the cells containing 100 µL of medium and kept for incubation at standard cell culture conditions for 3 hours. DMEM with Alamar blue was served as blank. The absorbance of medium was measured and subtracted the blank values from cells' absorbance value and the percentage of viability and significance were calculated.

Once the optimization for hypoxia drug concentration was achieved, 15,000 cells were seeded on a glass coverslip and allowed to grow for 70-80% confluent. 150 µM of $CoCl_2$ were used for the treatment for 24 hours in serum deprived medium. The cells deprived of serum but not exposed to stress for the same duration was used as control.

Quantitative Gene expression analysis by Real Time-PCR

Gene expression by PCR was done for characterizing the cultured retinal cells as well as to measure the expression of genes under hypoxia. In brief, the total RNA was extracted from the retinal cells before and after the stress induction by TRIzol method. Total RNA was reverse transcribed into cDNA using Verso cDNA synthesis Kit (ThermoFisher Scientific, Catalog No. AB1453B) according to the manufacture's protocol. The primer sequences used for conventional PCRs were given in the supplementary file Table S1. In order to quantify the average mRNA expression in the entire MRC population, we performed quantitative real time PCR (qRT) on Applied Biosystems 7900 HT system for a total reaction volume of 20 µL. Reaction mixture (10 µL) included iTaq™ Universal SYBR® Green Supermix (BIO-RAD, Catalog No. 172-5121), 200 nM of primer and cDNA. The relative measure of the concentration of target gene (CT) was calculated by using software SDS 2.4. Analysis of gene expression changes was done using $2^{-\Delta\Delta CT}$ method. Statistical analyses were performed using the $2^{-\Delta\Delta CT}$±SEM in three technical and biological replicates. The house keeping gene β-Actin was used as a normalizing control. The primer sequences used for quantitative real time PCRs are given in the supplementary file Table S2.

Protein Imaging and quantification

In order to assess the glial hyper reactivity under hypoxia, we plan to compare the protein expression in GFAP positive and IBA1 positive cells in control and stressed condition. In order to achieve this, we performed immunocytochemistry and quantitative protein imaging. Large scale imaging was performed using lasers with excitation at 405 nm, 488 nm and 594 nm for DAPI, Alexa 488 and Alexa 594 with Leica SP8 laser scanning confocal microscope with a 40X dry objective. In order to quantify the protein level in a large section of MRC, we acquired a panorama using mosaicking technique for a field of view (1.8 mm X 1.8 mm) containing 10 X 10 square sections (each section of dimension of 180 µm X 180 µm) with approximately 20% overlap. Hundred sections were stitched to obtain the spatial protein profiling for a large section by Leica LAS X Software. In order to show the representative images of GFAP and IBA1 expression under no stress and hypoxia 3D imaging was performed through acquiring Z-stack images along the z-axis (Total Z height = ~12 µm, Z- stack thickness between each slice = 0.5 µm) with a 63X oil immersed objective. The fluorescence intensity corresponding to various region of interest was acquired using Leica LAS X software. In order to quantify the glial reactivity in MRC, we further created a 3D surface plot of GFAP and IBA1 expression from the panorama images using ImageJ software.

Time-lapse Ca^{2+} imaging of the cells

In order to perform cytosolic calcium imaging, cells were loaded with 2 µM Fluo-4 (Molecular Probes, Life Technologies, Grand Island, NY) for 30 min in Hank's Balanced Salt Solution (HBSS) (Invitrogen, Life Technologies, Grand Island, NY). The cells were then washed thrice with HBSS followed by fluorescence imaging (Excitation: 488nm) at 37°C. Time-lapse movies were acquired every 10s, for 10 min and raw data were analyzed with Matlab (The MathWorks, Natick, MA). An image segmentation algorithm, based on principal component analysis, was optimized for automated segmentation of cells present in MRC. The maximum amplitude of Fluo-4 intensity and Ca^{2+} spike count was computed for control and hypoxia and were represented through boxplots. In order to perform the correction for the photobleaching effect, we used second order polynomial fitting and estimation of coefficients.

Data analysis

The time course of Ca^{2+} transients obtained for 600 seconds was analyzed using MATLAB. The analysis was performed for all the segmented cells obtained from the live imaging video for respective conditions. In order to quantify the activity level in MRC, we obtained the raster plot via peak identification from the time course of Fluo-4 intensity. Although the cell size has not been accounted to make any size-based correction, the Fluo-4 intensity was normalized with respect to basal level Fluo-4 intensity for each cell (Swain et al., 2018). We performed *k*-means clustering based on Ca^{2+} spike count and Ca^{2+}_{max} (maximum calcium amplitude) (number of cluster $k = 4$ for control condition). The automation in classification of cells yielded different types of cells, black and cyan-cells with lower activity, green-cells with moderate activity and red-cells with highest activity. Here, we report the cells with higher amplitude and spike count as the hyperactive cells and the cells with moderate amplitude and spike count as moderately active cells. Furthermore, we used the boundaries obtained from control condition as the reference to

classify the calcium transients under hypoxic condition. The relative percentage of four subpopulations were represented using stack bar plots. The dataset corresponding to control and hypoxia tested for normality using Jarque–Bera test. As the majority of dataset were not normally distributed, we have used Kruskal–Wallis test to study the effects of hypoxia on mixed retinal population. Statistical tests were performed at the significance level of 0.05. In box plots, the results were presented in terms of median, interquartile range, and whiskers 10–90%. We also performed Kruskal-Wallis test to check whether the percentages of cells corresponding to different clusters (having high, moderate, low and no activity) are significantly different in stressed condition compared to no stress condition.

Data sampling: In order to select data from multiple videos in an unbiased manner, 60% of the cells were randomly chosen from MRC population (Population size=160, sampling was repeated five times, size of each random sample = 90 cells) for clustering (Swain et al., 2018). All bar graphs were plotted to present mean±SEM. The schematic representation of data analysis is given in supplementary figure S9.

Results

Culturing of primary mixed retinal cells and characterization

The cells were heterogeneous in nature, which was evident from their morphology. The dissociated retinal cell cultures started to adhere after 3-4 days and became confluent within 3-4 weeks in culture. Most importantly, the cells were having both neuronal and glial morphology with a network of processes (Supplementary Figure S1 and Figure S2). Immunofluorescent staining and PCR characterization was done for glial as well as neural populations of the cultured cells. Immunofluorescence of the cells in MRC clearly showed positive staining for neuronal progenitor marker nestin (Figure 1A), Müller glial marker glutamine synthetase (GS) (Figure 1B), glial fibrillary acidic protein (GFAP) for astrocytes (Figure 1C) microglia marker IBA1 (Figure 1D), and β-III tubulin (Figure 1E) for neuronal population. Likewise, PCR based characterization of the cells also confirmed the expression of genes specific to glial cells, neural progenitor cells and mature neurons in the dissociated retinal culture (Figure 2).

Reproducibility of cell population in MRC

Further to ascertain the robustness of this culture system and reproducibility of the cell types obtained, we have calculated the percentage of each cell types with respect to total number of DAPI stained cells in each culture obtained from different cadaver retina samples. Figure 3 shows the stack bars representation of subpopulation percentages for each cell type in MRC corresponding to samples from four cadaver donor retinas. The result shows that the percentage of each cell type for the samples derived from different eye are not significantly different ($p > 0.05$) (Figure 3).

Cell viability under hypoxic stress

The cells were actively dividing until passage four and the earlier passage of the cells (P1 and P2) were used for the experiment. Prior to the experiment, a PCR based characterization was done for the cell specific genes to ensure all major glial cell types and mature neurons in the culture (Supplementary Figure S3). The serum deprived cells were exposed to different

concentrations of $CoCl_2$ for a time period of 24 hours and measured the cell viability by Alamar blue method. We have used a concentration range from 100 to 250 µM of $CoCl_2$. The cell viability of controls was always maintained as 100%. We have found a concentration dependent reduction of cell viability under hypoxic treatment. The results showed a significant reduction in cell viability when the cells were treated with 150 µM (62.33±1.71, $p<0.05$) (Figure 4).

Imaging of Ca^{2+} spiking in a mixed retina population

In order to evaluate the changes in intracellular calcium level under hypoxia, we first characterized the basal level cytosolic Ca^{2+} spiking in MRC. Figure 5A, B shows the time-lapse imaging of cytosolic Ca^{2+} in MRC under no stress condition (A movie file shows these details. Supplementary Movie S1). Next, we performed the time-lapse imaging of intracellular Ca^{2+} for hypoxia (Figure 5C and D, an additional movie file shows this details Supplementary Movie S2). The spatial mapping of single cell Fluo-4 intensity in MRC population showed the Ca^{2+} spiking in a single cell under various conditions. The heat map representation of time lapse Ca^{2+} responses provided prominent visualization of Ca^{2+} spiking (Figure 5B, D and Supplementary Figure S4). The time lapse videos were further processed by image segmentation algorithm to acquire data and the schematic diagram of data acquisition process were shown in supplementary figure S5. The Ca^{2+} spiking pattern under no stress and hypoxia (Figure 6A, B) indicated that the intracellular Ca^{2+} oscillates at variable frequencies for different cells in MRC population. Note that, each of the cell in the whole population did not show Ca^{2+} spiking indicating that there were some cells having relatively less activity.

In order to observe Ca^{2+} spiking pattern in large MRC population, we have plotted the raster plot for 160 cells (Figure 6C, D). Raster plot showed that there is an increase in Ca^{2+} spike count in case of hypoxia compared to no stress condition. This was further validated using boxplot representation(Figure 6E and F) showing the comparison of Ca^{2+} spike count and Ca^{2+}_{max} between no stress condition and hypoxia. The boxplot representation clearly indicated that hypoxia induces a significant increase in Ca^{2+} spike count in MRC population ($p<0.05$).

Classification of hypoxia mediated modulation of Ca^{2+} spiking

In order to obtain a subpopulation profiling of the calcium spiking pattern present in MRC population, we implemented the *k*-means clustering (Supplementary Figure S6) under no stress condition (Figure 7A). Since Ca^{2+} spike count and Ca^{2+}_{max} can be used to characterize the neuronal activity, we chose these two features to perform the clustering of calcium spiking over time. The result showed that the cells can be grouped into various categories, hyperactive cells (high spiking high amplitude >6 spikes in 10 minutes), cells with moderate activity (moderate amplitude moderate spiking,1-6 spikes per 10 minutes, $Ca^{2+}_{max}> 0.5$), cells with lower activity (low amplitude, moderate spiking, 0-6 spikes per10 minutes, $Ca^{2+}_{max}<0.5$). Using these boundary constraints corresponding to two features for each subpopulation of MRC under no stress condition, we performed the classification of the Ca^{2+} spiking under hypoxia (Figure 7B). Further we plotted the stack bars representing the relative percentages of each categories (Figure 7C). The percentage of hyperactive cells and cells with moderate activity were found to be higher in hypoxia compared to no stress condition ($p<0.05$) (Figure 7D). Moreover, the percentage of low active cells were significantly lower in case of hypoxia compared to control ($p<0.05$).

Further clustering of Ca^{2+} spiking of MRC under normal condition obtained from four donor retina was performed. Figure 8A shows the stack bars representing subpopulation profiles of Ca^{2+} spiking corresponding to cells from each donor retina. This analysis showed that the percentages of each subtype are not significantly different across patients (p> 0.05) (Figure 8B).

Quantitative gene expression analysis by Real Time PCR

Cells exposed 150 µM $CoCl_2$ in serum deprived medium to induce hypoxia and control cells were harvested after 24 hours and RNA was extracted. Real time PCR was performed for 3 sets of heterogeneous cell cultures derived from 3 different retina sources. The expression of representative genes from different pathways known to be involved in DR pathogenesis including hypoxia signaling (*HIF1-α, NERF2* and *OXR1*) inflammation (*IL-1β, IL-8* and *C3*), angiogenesis (*CXCR4* and *VEGF*) and apoptosis (*BAX* and *Caspase 3*) were measured (Out of 11 genes measured the expression of 6 genes were found to be significantly upregulated in hypoxia (Figure 9). These include genes such as *HIF1-α,* which was found to be significantly upregulated by 2.28±0.37 folds under hypoxia (p<0.05). Likewise, the genes involved in oxidative stress response such as *OXR1* and *NERF2* were upregulated under hypoxia (*OXR1*: 2.56±0.53, p<0.05, *NERF2*: 1.7±0.4, p<0.05). Further the angiogenic genes such as *VEGF* and *CXCR4* were upregulated 3.48±0.8; p<0.05 and 6.89±1.02; p<0.05 fold respectively. The expression of *IL-1β*- was found to be 15.3± 2.5; p<0.05 in hypoxia treated cells, even though the expression of other inflammatory genes such as *C3, IL-8* was found to be higher in hypoxic treatment, while these increase was not found to be significant (*C3*: 1.53±0.05; p>0.05, *IL-8*: 1.7±0.4, p>0.05). Likewise, the apoptotic markers *Caspase 3* and *BAX* showed an increased expression under hypoxia (*Caspase-3*: 2.26±0.63; p>0.05, *BAX*:1.41±0.3; p>0.05).

Quantitative analysis of IBA1 and GFAP at protein level under hypoxic condition in primary mixed retina culture

Next, we hypothesized that the expression of cell-type specific protein is increased in MRC population when subjected to hypoxia. Since significant spatial heterogeneity was observed for various proteins in MRC, the protein expression was quantified through a large-scale imaging using confocal microscope. To examine the hypoxic injury on microglia and astrocytes, we analyzed IBA1 and GFAP expression from the panorama images. Figure 10A, C shows the representative 3D images of IBA1 and GFAP positive cells chosen from MRC under hypoxic injury. In order to assess the glial reactivity, we constructed 3D surface plot corresponding to spatial profiling of IBA1 and GFAP under control and stress condition (Figure 10B, D).

The spatial pattern shows the differential expression of IBA1 and GFAP under stress compared to control condition indicating the activation of microglia and gliosis respectively under injury. Next, we performed the quantitative analysis of protein expression in large number of cells under each condition through boxplots (Figure 10E and F). The result suggests that hypoxia induces significant increase in IBA1 expression (2-fold) and GFAP (1.7-fold) (p<0.05). In addition to this, we also evaluated the protein expression of GS under hypoxic condition, however there was no significant difference (p>0.05; Kruskal–Wallis test) between control and hypoxic condition (Supplementary Figure S7). A double staining of GFAP and GS was also performed in retinal cells under control and hypoxic condition. This identified a clear

categorization of GFAP and GS positive cells in the culture (Supplementary figure S8) and upon treatment the GFAP level was found to be elevated in the cells and there was no change in the expression of GS.

Discussion

Glial cells are the supporting cells of the neural retina (Rubsam et al., 2018), and the homeostatic changes in the retina due to hypoxia or diabetes as seen in retinal vascular conditions like DR, ROP etc. affects these supporting cells, which eventually lead to neurotoxic consequences such as glutamate excitotoxicity caused by Müller glia dysfunction (Ishikawa, 2013), aberrant activation of microglia, astrogliosis, etc (Fischer et al., 2011). But there is a very little information available regarding the neuroglia interaction in the retina and their interaction during the progression of retinal vascular and neurodegenerative diseases. Ca^{2+} signaling being the major intrinsic signaling system in the glial cells, plays a vital role in angiogenesis, inflammation and most importantly neuroprotection in the retina (Vecino et al., 2016). Hence it is imperative to understand the changes in this intrinsic signaling system and their effect on neuronal damage under the stressed condition in a system that closely mimics human retina.

The current study explores the synergistic activity of neuron, Müller glia, astrocytes, and microglia in the mixed retinal culture under normal and stress conditions through clustering of calcium dynamics obtained from population-level calcium imaging, gene expression profiles as well as quantitative protein expression studies. The major finding of the present study is that the induction of hypoxia significantly modulates the Ca^{2+} pattern in MRC along with increase in IBA1 and GFAP level in microglia and in macroglial cells respectively.

Currently, with the advent of newer cellular and regeneration technologies, organoid cultures derived from iPSCs are more in focus for studying and modelling the complex retinal diseases. (Hallam et al., 2018). These organoid cultures can mimic the in-situ response and thereby provide a suitable platform for studying the complex cellular interactions and early developmental changes, however during the process of their development, they undergo extensive genetic manipulations. Additionally, it requires high maintenance cost and longer duration for developing organoids reproducibly (Ho et al., 2018). Most importantly, organoid derived from iPSCs lacks differentiation into essential retinal cell phenotypes including endothelial and microglial cells (Achberger et al., 2019). Since microglial cells are known to modulate the response to oxidative stress and injury, using IPSC's derived cellular model may not be appropriate for hypoxia studies. The proposed primary mixed culture system developed in this study therefore, provides an advantage over organoid based models, primarily owing to the no genetic manipulation, easy to work, cost effectiveness and most importantly having the major retinal cell types being represented uniformly and reproducibly across all the cultures. However, obtaining sufficient human retina tissue without any degenerative changes and within 24 hours in sterile conditions for culturing could be challenging.

In order to establish the *in vitro* model for studying neuron-glia interactions under hypoxic conditions, it is essential to study both neuron and glial cell types in close proximity so that they can interact with each other. Since the response to any stress/injury is a function of different cell types present, we optimized the culture conditions such that it enables simultaneous

growth of four cell types. Also, no trophic and other growth factors were added to selectively differentiate them into specific cell types. While it would have been worthwhile to have endothelial cells too in the same culture however the required conditions for the same made it difficult to have them cultured along with neuron and glial cell types. Due to lack of enough cells for a flow cytometry-based counting, the percentage of each cell types in different MRC culture were calculated (Figure 3) and found to be similar across cultures implying the robustness of this model. However, this cell type specific ratios may change post hypoxia induction based on response to hypoxia by each cell types. Further, we preferred to use cells only from early passages to maintain them close to original phenotype. The gene expression analysis and functionality imaging together show that the proposed mixed retinal culture obtained from human eye is robust and reproducible and has a potential to be used for drug screening.

HIF-1α is the key regulator mediating the responses to hypoxia. Under normal oxygen tension condition, HIF-1α protein turnover is very quick due to the action of prolyl hydroxylases, that promotes its binding to the Von Hippel–Lindau protein, ubiquitination, and subsequent proteosomal degradation. Exposure with cobalt chloride ($CoCl_2$), blocks the catalytic activity of prolyl hydroxylases leading to the stabilization and accumulation of the HIF-1α protein, thereby creating an intracellular hypoxia-like state (Cervellati et al., 2014). Stabilization of HIF-1 α typically promotes the synthesis of reactive oxygen species (ROS), that further based on their intracellular concentration, modulates the transcription of genes involved in cell proliferation, differentiation, and death (Shu et al., 2019). The major findings of the present study suggest that hypoxia plays a significant role in regulation of inflammation, cellular apoptosis and vascular changes as seen in ischemic complications of retina such as DR.

Since average protein expression across multiple cell types present in the mixed culture may not capture the changes present in specific cell types, we performed a quantitative imaging for microglia and macroglia using their specific marker protein IBA1 and GFAP respectively under control and stressed condition.The quantitative comparison of cytokine, apoptotic and inflammatory gene expression in mixed retinal culture upon the induction of hypoxic condition also showed an increased expression for the major known genes associated with DR pathogenesis (Kowluru and Odenbach, 2004; Yan and Su, 2014).

In order to identify the fraction of hyperactive and silent cells, *k*-means clustering of calcium spiking was performed (Swain et al., 2018).The clustering study shows that hypoxia induced an increase in percentage of hyper active cells. Since the Ca^{2+} spiking patterns obtained from the mixed culture were found to be highly heterogeneous, the basal level response in control condition was categorized into various types. However, it would be strategic to determine the individual Ca^{2+} spiking signature specific to neuron, astrocytes, Müller and microglia cells in the mixed retinal culture. This would require measuring of the calcium spiking in live cells using the Fluo-4 dye and stain the respective cell types with specific protein markers. Calcium imaging along with live markers for each cell type such as neurons and astrocytes may yield better information on cell specific responses in mixed retinal cells though homogenous transfection of primary cells remains a challenge (Peri and Nüsslein-Volhard, 2008; Guo et al., 2017). In our model, we observed a significant modification in functionality through classification of calcium spiking under stressed condition. However, future studies may include the investigation on the calcium channels and GPCRs involved in the process using channel inhibitor and GPCR targeting drugs. Further, measurement of glutamate and reactive oxygen species may provide us

insight into whether an excessive stimulation of glutamate receptors results in an uncontrolled intracellular Ca^{2+} flow in neurons as a consequence of oxidative stress.

In conclusion, we report that the proposed model based on human mixed retinal culture system provides a significant improvement over current *in vitro* models based on individual cells. Our *in vitro* model reproducibly showed underlying key pathological changes as seen in retina (Ca^{2+}activation and major signaling/pathways) under hypoxia mimicking diabetic retinopathy and other retinal vascular diseases. Further optimization of the culture conditions so as to include endothelial cells in this primary mixed retinal cell culture model is underway and would allow to investigate the neuromodulatory effects of glial cell on the angiogenesis in retina. Although 3D culture model may yield a better understanding of neurodegeneration (Park et al., 2018), the 2D study on mixed system subjected to stress conditions can be used for drug testing studies. Moreover, measurement of calcium spiking and classification can be used for estimation of the neuronal activity and underlying inflammation in the retina.

Acknowledgements

The authors thank the family members of the donors/patients for kindly donating the eyes for establishing retinal cultures and the staff at the Ramayamma International Eye Bank, L V Prasad Eye Institute, Hyderabad, India for their help in the collection of the donor eyes. In completing this work, IK was supported by DST-SERB, Ministry of science and Technology, Government of India (EMR/2016/007068), Department of Biotechnology, Government of India (BT/01/COE/06/02/10), Government of India, as well as Hyderabad Eye Research Foundation and LG, SJ and IK were supported by Department of Biotechnology (BT/PR/16582/BID/667/2016), Government of India. Sarpras Swain was supported through PhD fellowship of the Ministry of Human Resource and Development, Government of India. Establishment of cell culture, characterization, hypoxia analysis by qPCR and Calcium imaging was done as a part of PhD thesis of Shahna Shahulhameed and Calcium imaging data analysis algorithm was included in the thesis work of Sarpras Swain, submitted to University of Hyderabad and Indian Institute of Technology, Hyderabad, respectively where the online versions are not archived yet.

Authors 'contribution

IK and LG conceived the idea; IK and LG wrote the protocol; IK and LG served as principal investigator. SC, JC, MDT,RR, MJA, SJ and SC were co-investigators, SSH performed most of the cell culture work and data analysis, SV performed cell culture work, SS and NS performed analysis for the Ca^{2+} imaging data; SSH, SS, IK and LG analyzed the data and wrote the manuscript; and all authors revised the paper and approved the submitted version.

Conflict of interest

The authors declare that they have no conflict of interest.

Funding disclosure

In completing this work, IK was supported by DST-SERB, Ministry of science and Technology, Government of India (EMR/2016/007068), Department of Biotechnology, Government of India (BT/01/COE/06/02/10), as well as Hyderabad Eye Research Foundation and LG, SJ and IK were supported by Department of Biotechnology (BT/PR/16582/BID/667/2016), Government of

India. Sarpras Swain was supported through PhD fellowship of the Ministry of Human Resource and Development, Government of India.

Data availability statements

All data generated or analysed during this study are included in this published article and its supplementary information files.

Contribution to the Field Statement: Oxidative stress caused by reduced oxygen levels (hypoxia) in the retina leads to abnormal blood vessel growth and death of neuronal cells eventually causing loss of vision. Glial cells are known as the supporting cells to neurons in the retina that modulate the response under the hypoxia and prevent cell death. In this study, we have established primary mixed cultures of retina cells including neuron and glial from human donor retina for understanding their interactions under low oxygen stress. A simultaneous monitoring of neuronal and glial interaction in normal and stressed condition was achieved by studying the changes in genes involved in promoting inflammation and abnormal blood vessel growth and release of intracellular Ca^{2+} using fluorescent imaging. Our study observed a significant increase in the expression of the specific genes that cause blood vessel proliferation and inflammation and hypervariable changes in the intracellular Ca^{2+} release in the retina. Specifically, the proposed experimental platform containing mixed retinal cell culture under hypoxia can serve as an *in vitro* model for understanding the pathology of retinal neurodegenerative diseases such as Diabetic retinopathy and retinopathy of prematurity etc. This model can also be used to screen novel drug molecules to treat these retinal diseases

References

Acharya, N.K., Qi, X., Goldwaser, E.L., Godsey, G.A., Wu, H., Kosciuk, M.C., et al. (2017). Retinal pathology is associated with increased blood-retina barrier permeability in a diabetic and hypercholesterolaemic pig model: Beneficial effects of the LpPLA2 inhibitor Darapladib. *Diab Vasc Dis Res* 14(3)**,** 200-213. doi: 10.1177/1479164116683149.

Achberger, K., Probst, C., Haderspeck, J., Bolz, S., Rogal, J., Chuchuy, J., et al. (2019). Merging organoid and organ-on-a-chip technology to generate complex multi-layer tissue models in a human retina-on-a-chip platform. *Elife* 8. doi: 10.7554/eLife.46188.

Agte, S., Pannicke, T., Ulbricht, E., Reichenbach, A., and Bringmann, A. (2017). Two different mechanosensitive calcium responses in Muller glial cells of the guinea pig retina: Differential dependence on purinergic receptor signaling. *Glia* 65(1)**,** 62-74. doi: 10.1002/glia.23054.

Arden, G.B., and Sivaprasad, S. (2011). Hypoxia and oxidative stress in the causation of diabetic retinopathy. *Curr Diabetes Rev* 7(5)**,** 291-304.

Arroba, A.I., Alvarez-Lindo, N., van Rooijen, N., and de la Rosa, E.J. (2014). Microglia-Muller glia crosstalk in the rd10 mouse model of retinitis pigmentosa. *Adv Exp Med Biol* 801**,** 373-379. doi: 10.1007/978-1-4614-3209-8_47.

Barber, A.J., Antonetti, D.A., and Gardner, T.W. (2000). Altered expression of retinal occludin and glial fibrillary acidic protein in experimental diabetes. The Penn State Retina Research Group. *Invest Ophthalmol Vis Sci* 41(11)**,** 3561-3568.

Brahmachari, S., Fung, Y.K., and Pahan, K. (2006). Induction of glial fibrillary acidic protein expression in astrocytes by nitric oxide. *J Neurosci* 26(18)**,** 4930-4939. doi: 10.1523/JNEUROSCI.5480-05.2006.

Cervellati, F., Cervellati, C., Romani, A., Cremonini, E., Sticozzi, C., Belmonte, G., et al. (2014). Hypoxia induces cell damage via oxidative stress in retinal epithelial cells. *Free Radic Res* 48(3)**,** 303-312. doi: 10.3109/10715762.2013.867484.

Crish, S.D., and Calkins, D.J. (2011). Neurodegeneration in Glaucoma: Progression and Calcium-Dependent Intracellular Mechanisms. *Neuroscience* 176**,** 1-11. doi: 10.1016/j.neuroscience.2010.12.036.

Fischer, F., Martin, G., and Agostini, H.T. (2011). Activation of retinal microglia rather than microglial cell density correlates with retinal neovascularization in the mouse model of oxygen-induced retinopathy. *J Neuroinflammation* 8**,** 120. doi: 10.1186/1742-2094-8-120.

Guo, D., Zou, J., Rensing, N., and Wong, M. (2017). In Vivo Two-Photon Imaging of Astrocytes in GFAP-GFP Transgenic Mice. *PLoS ONE* 12(1)**,** e0170005. doi: 10.1371/journal.pone.0170005.

Hainsworth, D.P., Katz, M.L., Sanders, D.A., Sanders, D.N., Wright, E.J., and Sturek, M. (2002). Retinal capillary basement membrane thickening in a porcine model of diabetes mellitus. *Comp Med* 52(6)**,** 523-529.

Hallam, D., Hilgen, G., Dorgau, B., Zhu, L., Yu, M., Bojic, S., et al. (2018). Human-Induced Pluripotent Stem Cells Generate Light Responsive Retinal Organoids with Variable and Nutrient-Dependent Efficiency. *Stem Cells* 36(10)**,** 1535-1551. doi: 10.1002/stem.2883.

Hartung, T. (2008). Thoughts on limitations of animal models. *Parkinsonism Relat Disord* 14 Suppl 2**,** S81-83. doi: 10.1016/j.parkreldis.2008.04.003.

Ho, B.X., Pek, N.M.Q., and Soh, B.S. (2018). Disease Modeling Using 3D Organoids Derived from Human Induced Pluripotent Stem Cells. *Int J Mol Sci* 19(4). doi: 10.3390/ijms19040936.

Ibrahim, A.S., El-Remessy, A.B., Matragoon, S., Zhang, W., Patel, Y., Khan, S., et al. (2011). Retinal Microglial Activation and Inflammation Induced by Amadori-Glycated Albumin in a Rat Model of Diabetes. *Diabetes* 60(4)**,** 1122.

Ishikawa, M. (2013). Abnormalities in glutamate metabolism and excitotoxicity in the retinal diseases. *Scientifica (Cairo)* 2013**,** 528940. doi: 10.1155/2013/528940.

Kowluru, R.A., and Odenbach, S. (2004). Role of interleukin-1beta in the pathogenesis of diabetic retinopathy. *Br J Ophthalmol* 88(10)**,** 1343-1347. doi: 10.1136/bjo.2003.038133.

Kuchibhotla, K.V., Lattarulo, C.R., Hyman, B.T., and Bacskai, B.J. (2009). Synchronous hyperactivity and intercellular calcium waves in astrocytes in Alzheimer mice. *Science* 323(5918)**,** 1211-1215. doi: 10.1126/science.1169096.

Matteucci, A., Varano, M., Mallozzi, C., Gaddini, L., Villa, M., Gabrielli, S., et al. (2015). Primary Retinal Cultures as a Tool for Modeling Diabetic Retinopathy: An Overview. *BioMed Research International* 2015**,** 16. doi: 10.1155/2015/364924.

Newman, E.A. (2005). Calcium increases in retinal glial cells evoked by light-induced neuronal activity. *J Neurosci* 25(23)**,** 5502-5510. doi: 10.1523/JNEUROSCI.1354-05.2005.

Park, J., Wetzel, I., Marriott, I., Dréau, D., D'Avanzo, C., Kim, D.Y., et al. (2018). A 3D human triculture system modeling neurodegeneration and neuroinflammation in Alzheimer's disease. *Nature Neuroscience* 21(7)**,** 941-951. doi: 10.1038/s41593-018-0175-4.

Pereira Tde, O., da Costa, G.N., Santiago, A.R., Ambrosio, A.F., and dos Santos, P.F. (2010). High glucose enhances intracellular Ca2+ responses triggered by purinergic stimulation in retinal neurons and microglia. *Brain Res* 1316**,** 129-138. doi: 10.1016/j.brainres.2009.12.034.

Peri, F., and Nüsslein-Volhard, C. (2008). Live Imaging of Neuronal Degradation by Microglia Reveals a Role for v0-ATPase a1 in Phagosomal Fusion In Vivo. *Cell* 133(5)**,** 916-927. doi: 10.1016/j.cell.2008.04.037.

Puro, D.G. (2002). Diabetes-induced dysfunction of retinal Müller cells. *Transactions of the American Ophthalmological Society* 100**,** 339-352.

Rohowetz, L.J., Kraus, J.G., and Koulen, P. (2018). Reactive Oxygen Species-Mediated Damage of Retinal Neurons: Drug Development Targets for Therapies of Chronic Neurodegeneration of the Retina. *Int J Mol Sci* 19(11). doi: 10.3390/ijms19113362.

Rosa, J.M., Bos, R., Sack, G.S., Fortuny, C., Agarwal, A., Bergles, D.E., et al. (2015). Neuron-glia signaling in developing retina mediated by neurotransmitter spillover. *Elife* 4. doi: 10.7554/eLife.09590.

Rubsam, A., Parikh, S., and Fort, P.E. (2018). Role of Inflammation in Diabetic Retinopathy. *Int J Mol Sci* 19(4). doi: 10.3390/ijms19040942.

Shin, E.S., Huang, Q., Gurel, Z., Sorenson, C.M., and Sheibani, N. (2014). High glucose alters retinal astrocytes phenotype through increased production of inflammatory cytokines and oxidative stress. *PLoS One* 9(7)**,** e103148. doi: 10.1371/journal.pone.0103148.

Shu, S., Wang, Y., Zheng, M., Liu, Z., Cai, J., Tang, C., et al. (2019). Hypoxia and Hypoxia-Inducible Factors in Kidney Injury and Repair. *Cells* 8(3). doi: 10.3390/cells8030207.

Skytt, D.M., Toft-Kehler, A.K., Br, #xe6, ndstrup, C.T., Cejvanovic, S., et al. (2016). Glia-Neuron Interactions in the Retina Can Be Studied in Cocultures of Müller Cells and Retinal Ganglion Cells. *BioMed Research International* 2016**,** 10. doi: 10.1155/2016/1087647.

Swain, S., Gupta, R.K., Ratnayake, K., Priyanka, P.D., Singh, R., Jana, S., et al. (2018). Confocal imaging and k-means clustering of GABAB and mGluR mediated modulation of Ca2+ spiking in hippocampal neurons. *ACS Chem Neurosci*. doi: 10.1021/acschemneuro.8b00297.

Vecino, E., Rodriguez, F.D., Ruzafa, N., Pereiro, X., and Sharma, S.C. (2016). Glia-neuron interactions in the mammalian retina. *Prog Retin Eye Res* 51**,** 1-40. doi: 10.1016/j.preteyeres.2015.06.003.

Yan, H.T., and Su, G.F. (2014). Expression and significance of HIF-1 alpha and VEGF in rats with diabetic retinopathy. *Asian Pac J Trop Med* 7(3)**,** 237-240. doi: 10.1016/S1995-7645(14)60028-6.

Yu, Y., Chen, H., and Su, S.B. (2015). Neuroinflammatory responses in diabetic retinopathy. *J Neuroinflammation* 12**,** 141. doi: 10.1186/s12974-015-0368-7.

Zhao, L., Zabel, M.K., Wang, X., Ma, W., Shah, P., Fariss, R.N., et al. (2015). Microglial phagocytosis of living photoreceptors contributes to inherited retinal degeneration. *EMBO Mol Med* 7(9)**,** 1179-1197. doi: 10.15252/emmm.201505298.

Figure 1. Immunofluorescence based characterization of human primary mixed retinal cells. The representative images clearly show the presence of neurons and all type of glial cells (**A**) cells expressing neuronal progenitor marker; Nestin (**B**) cells expressing Müller glia marker; GS (**C**) cells expressing astrocytes marker; GFAP (**D**) cells expressing microglial marker; IBA1 and (**E**) cells expressing neuronal marker; β-III tubulin (Magnification, 20X, Scale bar- 200 µm).

Figure 2. PCR based characterization for cell type specific markers; *GS, IBA1*, *β-III tubulin, GFAP* and *nestin* respectively, 1- DNA ladder, 2. positive control (Retina) and 3- Mixed retinal cells (MRC).

Figure 3. Analysis of model robustness in primary mixed retinal cultures obtained from different retinal tissues. The subpopulation percentages of four different cell types in MRC corresponding to samples from four retinal sources were calculated and percentage of each cell types are represented in the bar graph.

Figure 4. The mixed retinal cultures were treated with increasing concentration of $CoCl_2$for a period of 24 hrs. The viability was measured using Alamar blue based dose dependent cell viability assay (N=3 biological and technical replicates). The data are represented as Mean±SEM (n=3), N.S.- not significant, *p<0.05.

Figure 5. Fluorescent imaging of time course of cytosolic Ca^{2+} in human primary mixed retinal cells; representative time-lapse images for (**A**) control (no stress) (**C**) hypoxia (150 µM $CoCl_2$) (Magnification 20X, scale bar 200 µm). Representative spatial intensity mapping of Ca^{2+} flux in single cell present in MRC (**B**) control (**D**) hypoxia. The results clearly identified intracellular Ca^{2+} oscillates at variable frequencies for different cells in MRC population (Scale bar 20 µm).

Figure 6. Representative raw plots of time course of cytosolic Ca^{2+} under (**A**) no stress (**B**) hypoxia. The X-axis represents the change in fluorescence (ΔF/F0) and Y-axis represents the time course of experiments. The results clearly identified intracellular Ca^{2+} oscillation at variable frequencies for different cells in the MRC population. Raster plot representing the network activity in MRC (**C**) control, (**D**) hypoxia (n=160). Raster plot showed that there are cells with higher number of Ca^{2+} spike count in case of hypoxia compared to no stress condition.

Comparison of (**E**) Ca^{2+} spike count and (**F**) $Ca^{2+}{}_{max}$ between no stress condition and hypoxia. Data was presented using a box plot (*p<0.05; Kruskal-Wallis test)

Figure 7. Hypoxia modulates the clustering pattern of Ca^{2+} spiking in MRC. Clustering pattern under (**A**) no stress (number of clusters, k=4). (**B**) Classification of Ca^{2+} spiking under hypoxia. (**C**) Stack bars representing the subpopulation profiling of Ca^{2+} spiking corresponding to no stress and hypoxia. (**D**) Comparison of relative percentages of four clusters corresponding to no stress and hypoxia condition. The clustering was performed based on two features, Ca^{2+} spike count and $Ca^{2+}{}_{max}$. (Red- Hyperactive cells, Green- Cells with moderate activity, Black and Cyan- cells with lower activity, *p<0.05; Kruskal–Wallis test. N.S: not significant.

Figure 8. (**A**) Stack bar representation of sub-population profiles of Ca^{2+} spiking corresponding to samples from four donor retinas (**B**) Comparison of average relative percentages of various clusters across samples from four donor retinas (Number of cells taken from each sample corresponding to single donor tissue = 160; (*p<0.05; Kruskal-Wallis test) N.S. = Not significant)

Figure 9. Real-time Quantitative PCR analysis for genes involved in oxidative stress angiogenesis and inflammation and angiogenesis under hypoxia condition. The data are represented as Mean ± SEM(N=3). N.S: .not significant, *p<0.05, ***p<0.001; Kruskal–Wallis test.

Figure 10. Hypoxia alter the spatial profiling of IBA1 expression in MRC (**A**) Representative 3D images and (**B**) Surface plot showing IBA1 expression under no stress, hypoxia (ΔI indicating the fluorescent intensity corresponding to protein level) (**C**) Representative 3D images and (**D**) Surface plot showing the spatial profiling of GFAP expression under no stress and hypoxia. Quantitative analysis of protein expression was done in large number of cells under each condition, represented in box plot. (**E**) Comparison of IBA1 and (**F**) GFAP expression between no stress and hypoxia. *p<0.05. N.S: not significant; Kruskal–Wallis test.

Supplementary Figure 1. Representative phase contrast images of cells cultured from retina of human cadaveric/enucleated eyes. (**A**) Morphology of the cells after 4th, 8th and 16th days of culture at P0 stage. The cells showing the characteristic morphology of glial and neuronal type cells at day 16 confirm the heterogeneous retinal cell types in culture. (**B**) Morphology of cells in the MRC at 1st, 2nd and 3rd passages confirming the culture system is able to maintain these heterogeneous populations until 3rd passage (Magnification 10X, Scale bar 200µm).

Supplementary Figure 2. Representative immunofluorescent images of cells in Mixed retinal culture. The images clearly showing interaction of different cell types in the developed culture system. Panel showing the co-staining of (a)vimentin (Müller glia) and GFAP (Astrocytes), (b) IBA-1 (Microglia) and GS (Müller glia), (c) β-III tubulin (Neurons) and GFAP (Astrocytes), (d) GS (Müller glia) and GFAP (Astrocytes) (Magnification 20X, scale bar, 200 µm).

Supplementary Figure 3: Gene expression of neuron and glial cell specific markers from three different retinal donors' tissue at P1 and P2 passages, (A, B and C represents cells cultured from three different retinal tissues and 1 & 2 represents P1 and P2 passages)

Supplementary Figure 4: Time lapse images of the spatial intensity mappings of cytosolic calcium transients in human primary mixed retinal culture (**A**) no stress (**B**) hypoxia (Magnification 20X, Scale bar 200µm)

Supplementary Figure 5: Workflow representing various steps consisting of data acquisition, automated cell segmentation, cell labeling and data processing from the raw time-lapse videos.

Supplementary Figure 6: k-means clustering of Ca^{2+} spiking in control MRC (**A**) Raster plots representing the network activity in MRC (**B**) Clustering of Ca^{2+} spiking train in a MRC population using two features, Ca^{2+} spike-count and maximum Ca^{2+} spiking amplitude ($Ca^{2+}{}_{max}$) (**C**) Raster plot showing the clustering pattern in MRC population (**D**) Identification of optimal number of clusters for the Ca^{2+} spiking train using Davies-Bouldin index

Supplementary Figure 7: (**A**) GS expression in MRC under no stress and hypoxia (**B**) Surface plot showing GS expression under no stress and hypoxia (**C**) Comparison of GS expression between no stress and hypoxia. N.S.: not significant.

Supplementary Figure 8: Representative immunofluorescent images of GS and GFAP in cells under (a) control and (b) hypoxic conditions. (Magnification, 20X, Scale bar- 200 µm).

Supplementary Figure 9. A flow chart describing the detatiled summary of the Ca^{2+} imaging data analysis.

Supplementary Table S1. Nucleotide sequences of primers used in conventional PCR

Supplementary Table S2. Nucleotide sequences of primers used in quantitative Real time PCR

Supplementary video, Movie S1-S2: Measurement of intracellular Ca^{2+} transient in MRC using EVOS microscope (magnification 20X). Movie files show the Ca^{2+} spiking corresponding to no stress level (Movie S1) and Hypoxia (Movie S2) Spiking response was measured for 600 sec.

Figure 01.TIF

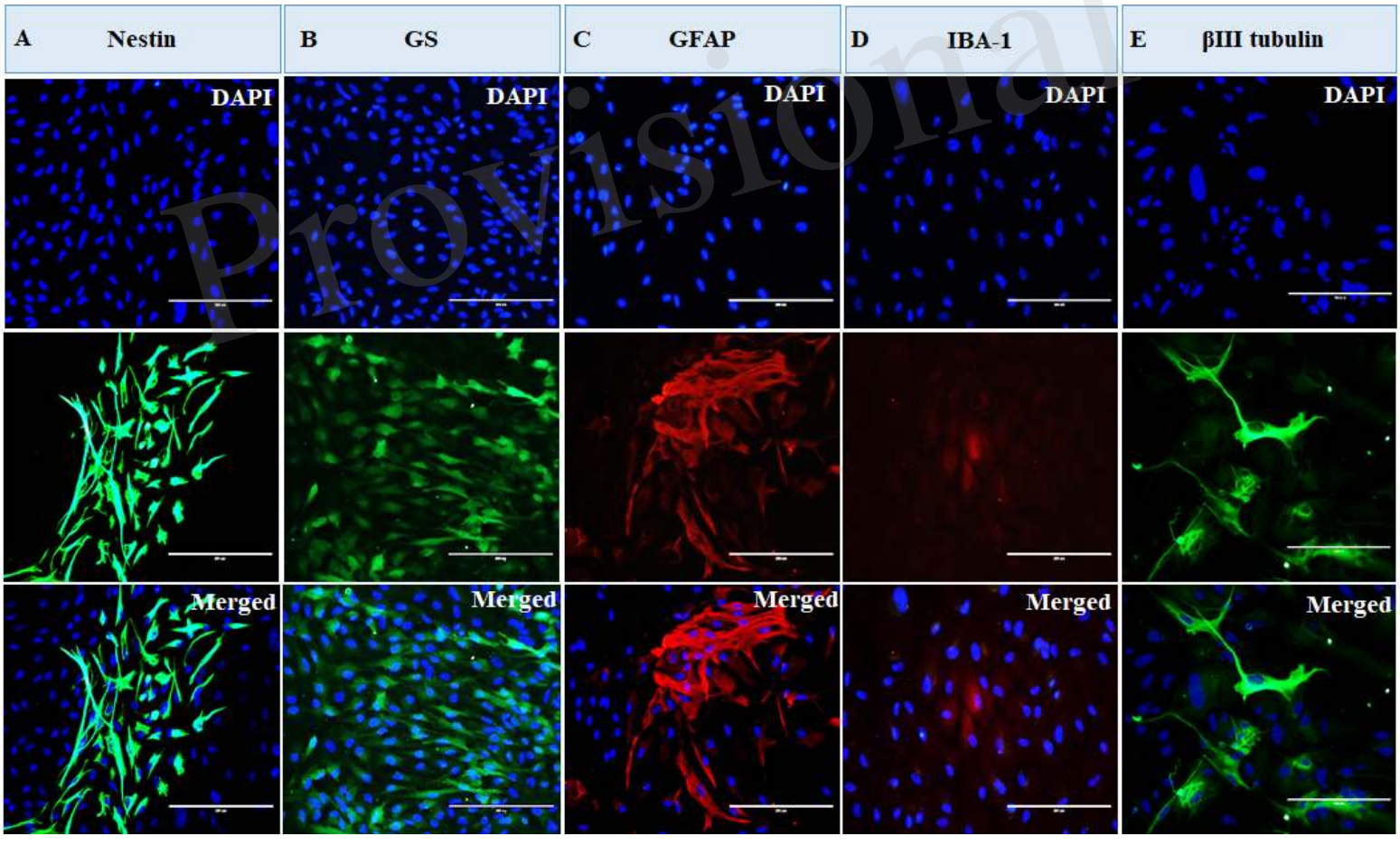

Figure 02.TIF

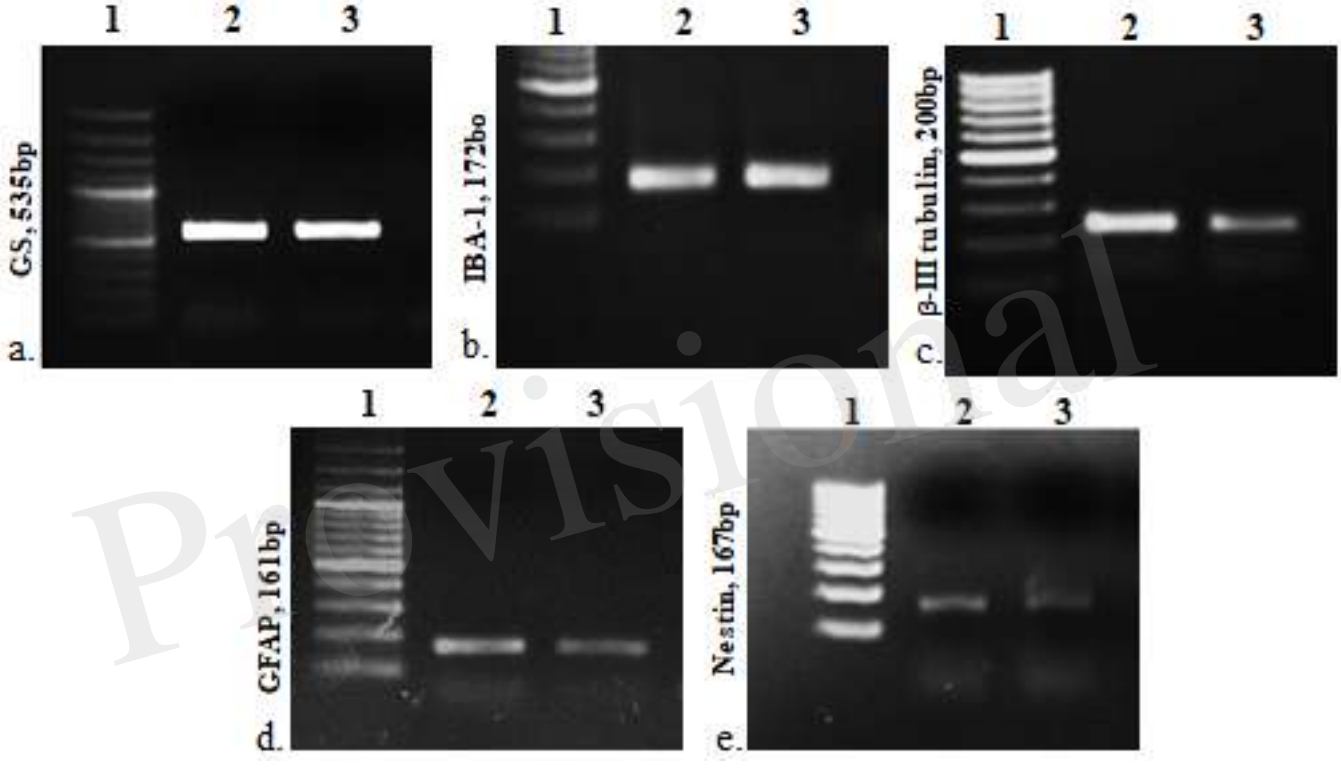

Figure 03.TIF

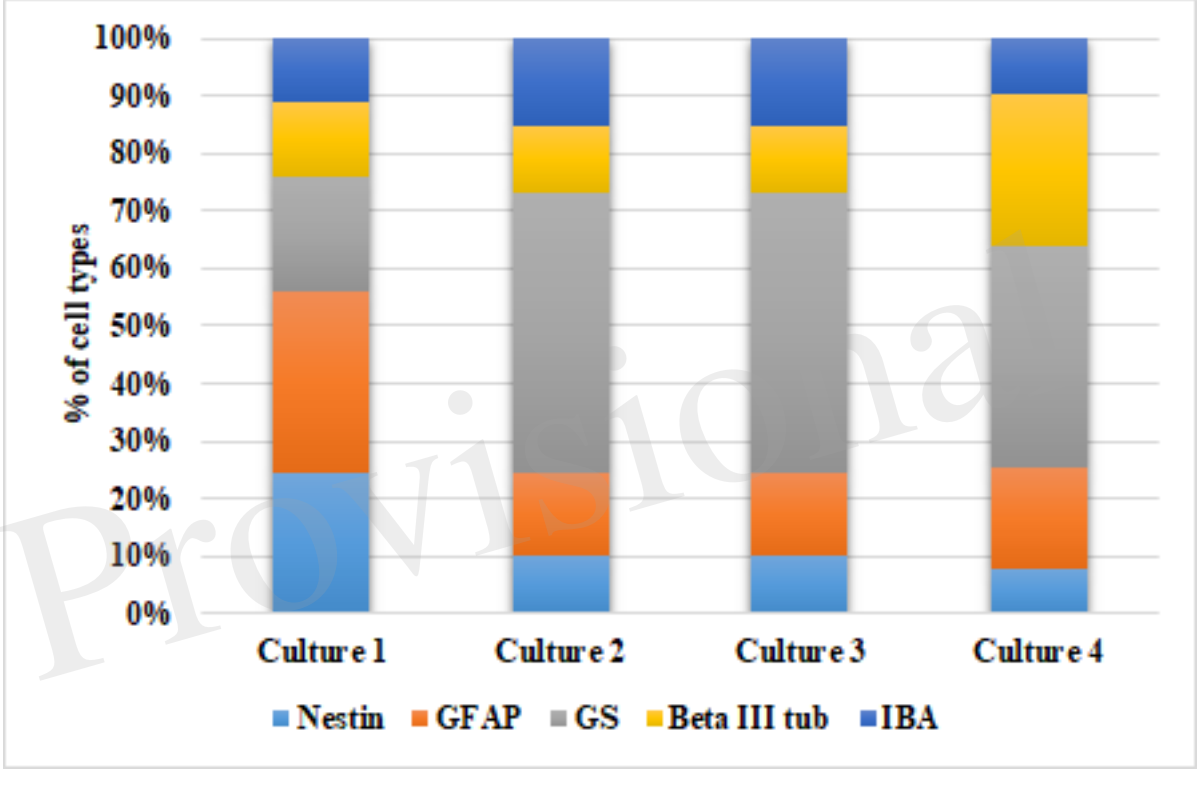

Figure 04.TIF

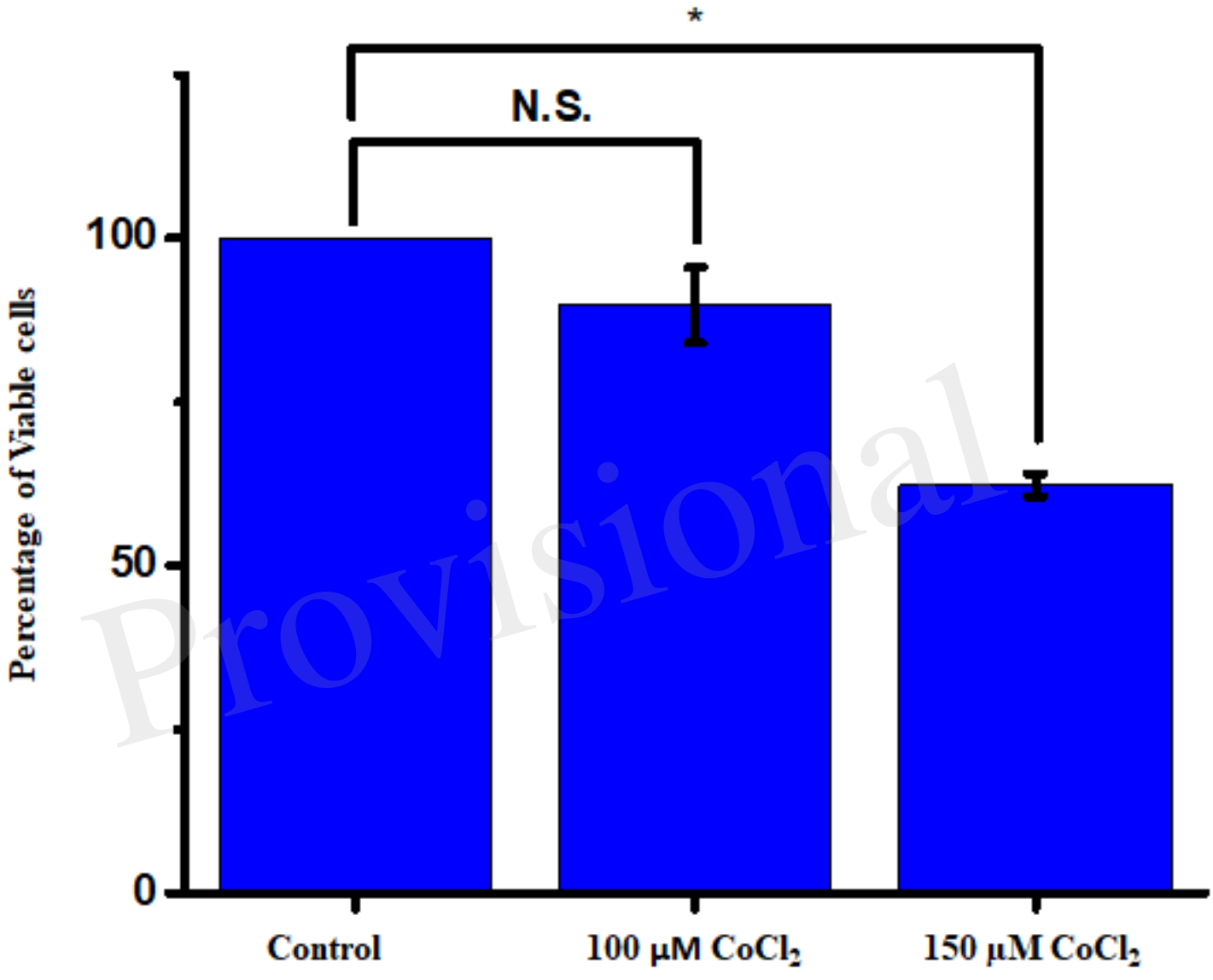

Figure 05.TIF

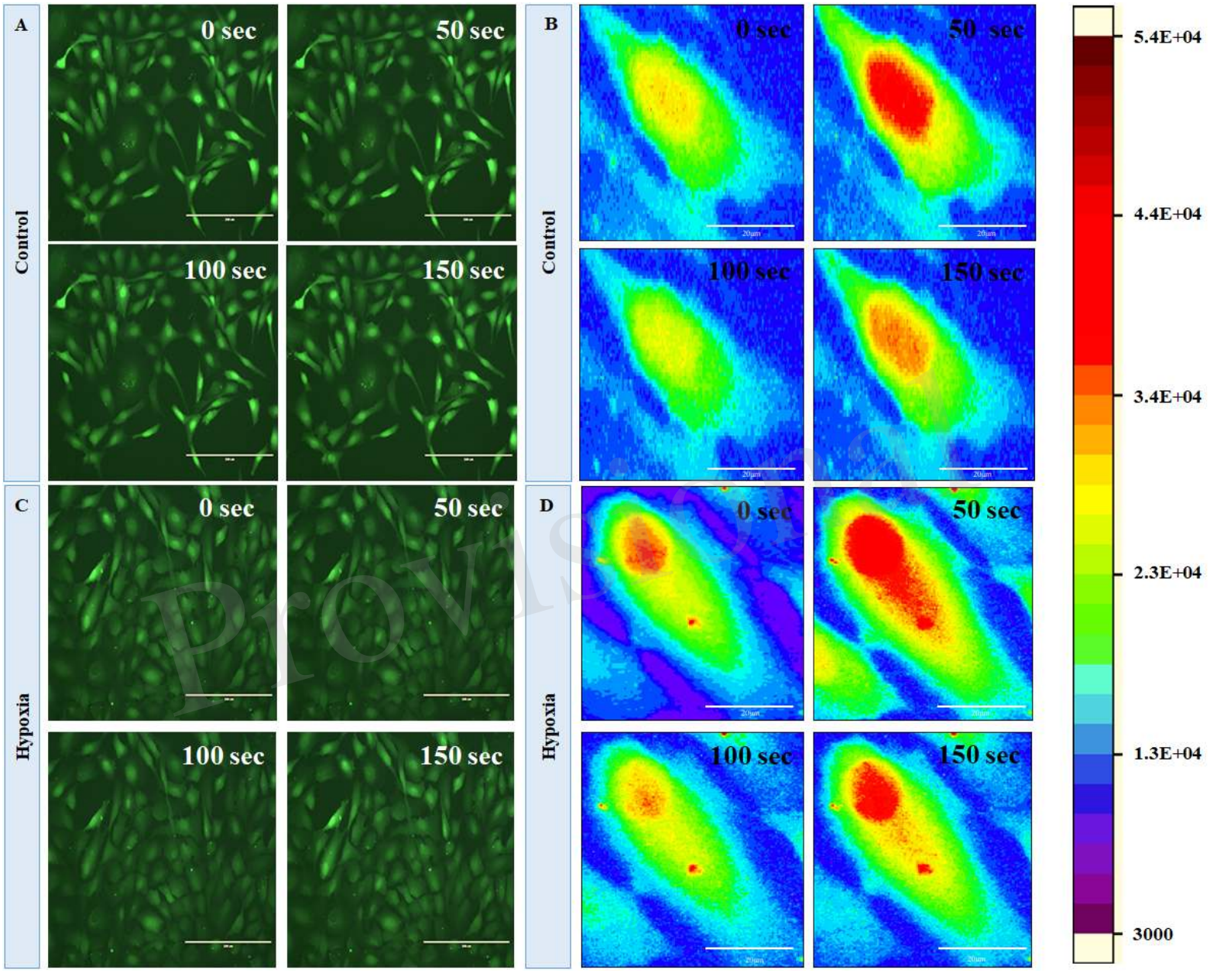

Figure 06.TIF

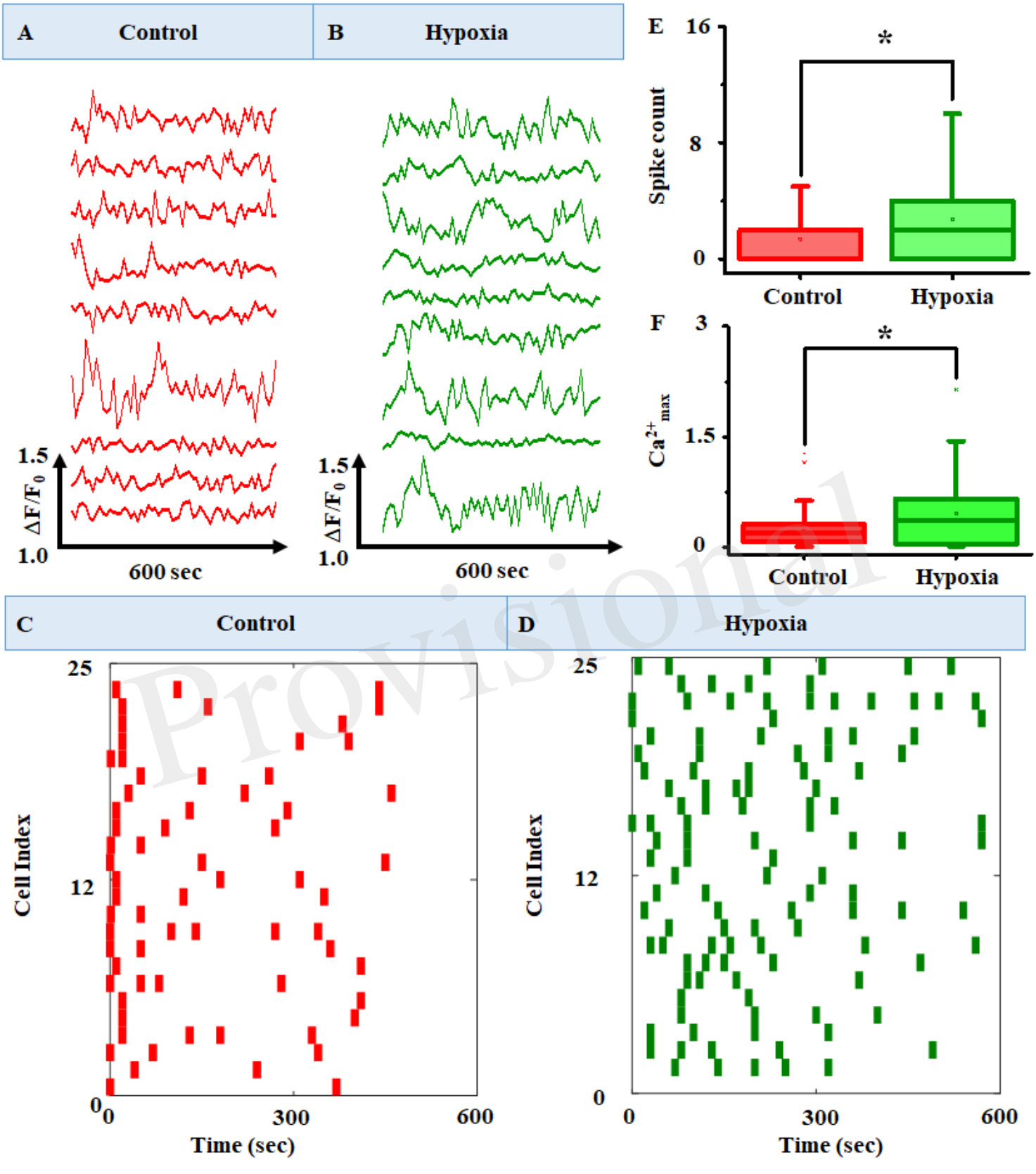

Figure 07.TIF

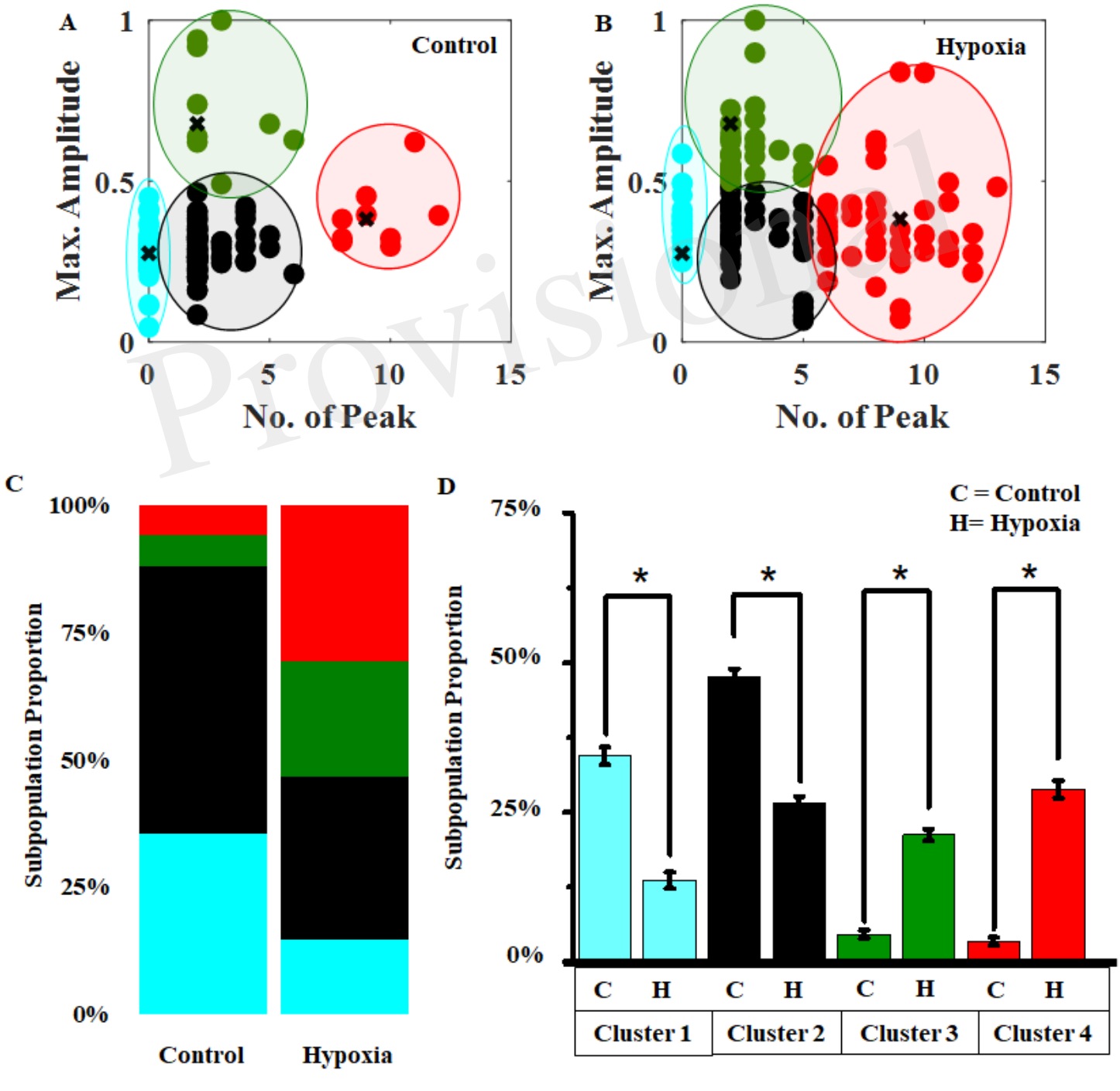

Figure 08.TIF

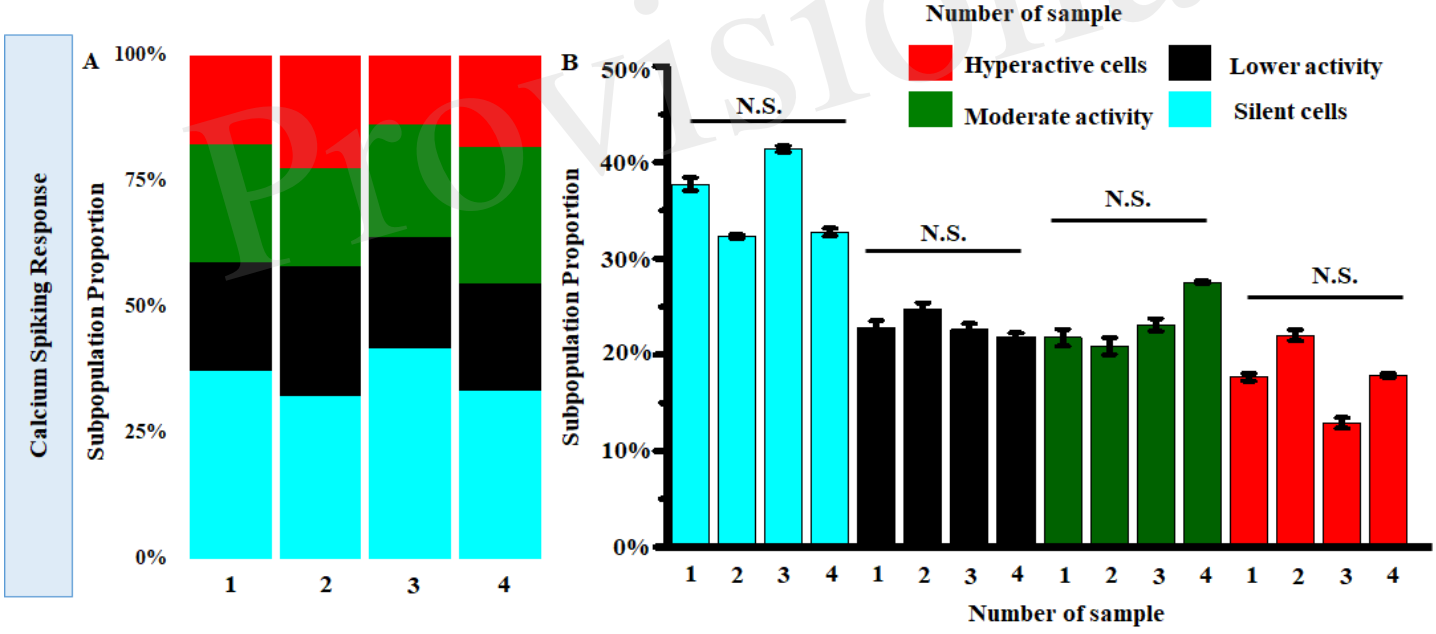

Figure 09.TIF

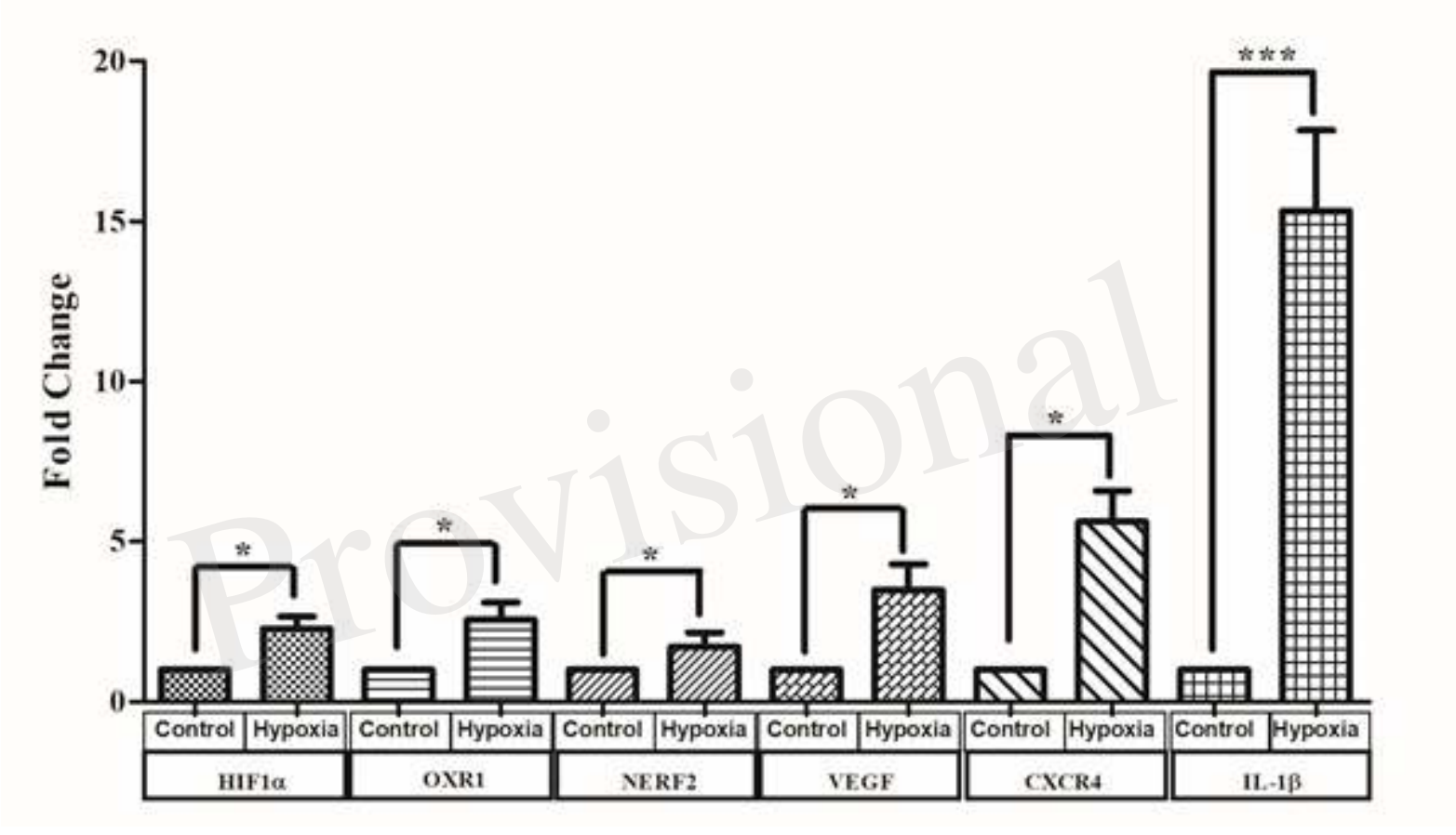

Figure 10.TIF